Available online at www.sciencedirect.com
SCIENCE DIRECT
Journal of Photochemistry and Photobiology A: Chemistry 176 (2005) 162–171
Journal of Photochemistry and Photobiology A:Chemistry
www.elsevier.com/locate/jphotochem

# Experimental and theoretical studies of the kinetics of the reactions of OH and OD with acetone and acetone-$d_6$ at low pressure

M.E. Davis [1], W. Drake, D. Vimal, P.S. Stevens *

*Environmental Science Research Center, School of Public and Environmental Affairs and Department of Chemistry, Indiana University, 1315 E. 10th Street, Bloomington, IN 47405, USA*

Available online 23 September 2005

**Abstract**

The kinetics of the reactions of OH and OD with acetone and acetone-$d_6$ were studied from 2–5 Torr and 258–402 K using a discharge flow system with laser induced fluorescence or resonance fluorescence detection of the OH radical. The rate constants at 300 K for the reaction of OH with acetone and acetone-$d_6$ were $(1.73 \pm 0.06) \times 10^{-13}$ and $(3.36 \pm 0.32) \times 10^{-14}$ cm$^3$ molecule$^{-1}$ s$^{-1}$, respectively. The rate constants at 300 K for the reaction of OD with acetone and acetone-$d_6$ were $(2.87 \pm 0.22) \times 10^{-13}$ and $(3.69 \pm 0.12) \times 10^{-14}$ cm$^3$ molecule$^{-1}$ s$^{-1}$, respectively. Above room temperature, the temperature dependence of the rate constants for the OH + acetone and acetone-$d_6$ display Arrhenius behavior and are described by the equations $k_H(T) = (3.92 \pm 0.81) \times 10^{-12}$ exp$(-938 \pm 70/T)$ and $k_D(T) = (8.19 \pm 1.45) \times 10^{-12}$ exp$(-1647 \pm 58/T)$ cm$^3$ molecule$^{-1}$ s$^{-1}$ for acetone and acetone-$d_6$, respectively. Measurements of $k_H$ and $k_D$ below room temperature begin to display non-Arrhenius behavior, consistent with previous measurements at higher pressures. Theoretical calculations of the kinetic isotope effect as a function of temperature are in good agreement with the experimental measurements using a hydrogen abstraction mechanism that proceeds through a hydrogen-bonded complex.


*Keywords:* Hydroxyl radical; Acetone; Kinetics; Isotope effect; Atmospheric chemistry

## 1. Introduction

Acetone is an important compound in the troposphere with a source strength of approximately 40–95 Tg yr$^{-1}$, with concentrations of 0.1 to 1 ppb in the free troposphere [1–3]. With a lifetime of 10–30 days based on photolysis and reaction with the OH radical, acetone can have a significant impact not only on local air quality, but also on global tropospheric ozone concentration and upper tropospheric chemistry [4]. In the upper troposphere, where the concentration of water molecules is low, acetone is also thought to be a major source of the OH radical, in some cases accounting for 50% of the total $HO_x$ concentration [4]. In the lower troposphere, the reaction with the OH radical is the major removal pathway.

The OH + acetone reaction can occur either by the abstraction of a hydrogen atom or by the addition of the OH radical to the carbonyl group (reactions (1) and (2)):

$$CH_3COCH_3 + OH \rightarrow CH_2C(O)CH_3 + H_2O \quad (1)$$

$$CH_3COCH_3 + OH \rightarrow CH_3C(O)OH + CH_3 \quad (2)$$

These radical products undergo subsequent reactions resulting that can lead to the net formation of OH radicals. In order to accurately predict the $HO_x$ formation rate from acetone and the fate of acetone in the troposphere, it is important to know the overall rate constant for the OH + acetone reaction and the branching ratio for reactions (1) and (2).

Previous measurements of the rate constant for the reaction of acetone with the hydroxyl radical using both absolute and relative rate techniques [5–14] have generally showed that the rate constant follows Arrhenius behavior between 240 and 400 K [10,11,13,14]. However, recent measurements have revealed that at upper tropospheric temperatures the rate constant displays non-Arrhenius behavior, becoming independent of temperature below 260 K [10,13].

The non-Arrhenius behavior of the OH + acetone reaction had been hypothesized by Wollenhaupt et al. [10] as a shift in the mechanism from primarily H-abstraction at high tem-

* Corresponding author. Tel.: +1 812 855 0732
*E-mail address:* pstevens@indiana.edu (P.S. Stevens).
[1] Present address: Aeronomy Laboratory, National Oceanic and Atmospheric Administration, 325 Broadway, Boulder, CO 80305, USA.

1010-6030/$ – see front matter © 2005 Elsevier B.V. All rights reserved.
doi:10.1016/j.jphotochem.2005.08.030

perature (∼90% at 400 K) to 50% each H-abstraction and OH-addition at 280 K, and to primarily OH-addition at lower temperatures (∼90% addition at 210 K) (reactions (1) and (2)). A branching ratio of 0.5 at 298 K had been inferred from experiments conducted by Wollenhaupt and Crowley [11], who measured the production of the methyl radical ($CH_3$), which is the expected product from the addition mechanism (reaction (2)), while Vasvari et al. [12] measured the 1-methylvinoxy radical ($CH_2C(O)CH_3$) formed from the abstraction mechanism (reaction (1)). Wollenhaupt and Crowley [11] also found evidence that the branching ratio for the addition mechanism decreased with temperature to 0.3 at 233 K.

In contrast, Vandenberk et al. [15] found no significant production of acetic acid from reaction (2), consistent with transition state theory and RRKM —master equation calculations demonstrating that the barrier for OH addition is significantly greater than that for hydrogen abstraction. Tyndall et al. [16] also found no evidence for direct formation of acetic acid from reaction (2). Similar results were reported by Talukdar et al. [17], who measured a yield for the acetonyl radical of $(96 \pm 11)\%$, independent of temperature between 237 and 353 K, and found that the yield of acetic acid from the reaction was less than 1%. Turpin et al. [18] also measured the yield of the acetonyl radical (relative to the acetonyl radical yields from the F + acetone and Cl + acetone reactions), suggesting a yield for reaction (1) between 80 and 100% at 298 K. Theoretical studies by Masgrau et al. [19] are also consistent with these results, suggesting that the acetic acid yield is less than 2% and decreases with temperature. Recent measurements by Raff et al. [20] using online mass spectrometry are also consistent with a yield of acetic acid of approximately 3% from the OH + acetone reaction, but measurements of the production $CD_3COOH$ from the OH + acetone-$d_6$ reaction resulted in a measured yield of approximately 18% at 298 K that increased with decreasing temperature.

Gierczak et al. [13] studied the OH + acetone and OH + acetone-$d_6$ reactions as well as the $^{18}$OH + acetone, the OD + acetone, and the OD + acetone-$d_6$ reactions as a function of temperature. They found a large primary kinetic isotope effect for the OH + acetone and OH + acetone-$d_6$ reactions, indicating that the reaction mechanism primarily involves hydrogen abstraction even at low temperatures. Talukdar et al. [17] measured the rate constant for the OH + acetone reaction at pressures of 1–3 Torr as a function of temperature, and found that the rate constant did not exhibit a significant pressure dependence, consistent with a hydrogen abstraction reaction. Farkas et al. [21] also measured the kinetic isotope effect at low pressure, finding value of $5.33 \pm 0.41$ at 298 K, consistent with measurements at higher pressure.

Based on the large primary kinetic isotope effect measured at low temperatures, Gierczak et al. [13] suggested that the formation of a pre-reactive addition complex in the hydrogen abstraction mechanism could explain the non-Arrhenius behavior rather than a shift in the mechanism from abstraction to addition, similar to that proposed for the OH + $HNO_3$ reaction [22]. Theoretical calculations of the kinetic isotope effect using variational transition state theory by Yamada et al. [14] using a mechanism similar to that of Gierczak et al. were able to reproduce the observed kinetic isotope effect for wide range of temperatures. However, the theoretical calculations overestimated the observed kinetic isotope effect at temperatures below 250 K, predicting an isotope effect greater than 10 at 200 K. Farkas et al. suggest that such a mechanism might lead to a kinetic isotope effect as high as 10, similar to that observed for the OH reactions with $HNO_3$ and $DNO_3$, and that the observed kinetic isotope effect of approximately 5–6 is not inconsistent with a mechanism that involves both addition and abstraction [21]. Unfortunately, there have been fewer measurements of the rate constant for the OH + acetone-$d_6$ reaction, especially at temperatures below 300 K.

This paper examines the kinetics of the OH + acetone and acetone-$d_6$ reactions at 2–5 Torr and 258–402 K. In addition, the room temperature rate constants for the OD + acetone and acetone-$d_6$ reactions were also measured. These are the first measurements of the temperature dependence of the kinetic isotope for this reaction at pressures less than 10 Torr. Results of ab initio calculations of the energetics of the intermediates and transition states for the OH + acetone and OH + acetone-$d_6$ reactions were used in conjunction with unimolecular rate theory to calculate the kinetic isotope effect as a function of temperature and determine if the observed kinetic isotope effect is consistent with a mechanism for this reaction involving hydrogen abstraction through an intermediate complex.

## 2. Experimental methods

Experiments were conducted using the discharge-flow (DF) technique using either resonance fluorescence (RF) or laser induced fluorescence (LIF) detection of the OH radicals. The experimental systems are similar to those described previously [23]. The reactor is a jacketed 100 cm long, 25 mm internal diameter Pyrex glass tube to which ports that allow the addition of gases are attached. A movable injector (3 mm o.d.) inserted into the flow-tube is used for the introduction of acetone and acetone-$d_6$. The injector and all areas of the flow-tube exposed to radicals were coated with halocarbon wax (Halocarbon Corporation) to reduce the loss of radicals on the reactor walls. Bulk flow velocities of 9.4–10.7 m s$^{-1}$ were achieved at 300 K using a Leyland D16B mechanical pump downstream of the detection zone. The reaction temperature was varied by circulating heated silicone oil or liquid nitrogen cooled ethanol through the jacket of the flow-tube. The temperature was monitored using a thermocouple located in the center of the reaction zone. Helium, used for the bulk flow gas, was introduced into the system by a MKS 1179 flow controller. The reactor pressure was measured in the reaction zone by a MKS Baratron capacitance manometer.

OH radicals were produced using the H + $NO_2$ → OH + NO reaction ($k^{II} = 1.3 \times 10^{-10}$ cm$^3$ molecule$^{-1}$ s$^{-1}$). H atoms were produced from a microwave discharge (Opthos Instruments Inc., model MPG-4) of $H_2$ in He. $NO_2$ ($(2–6) \times 10^{13}$ molecules cm$^{-3}$) was added in excess 2 cm upstream of the radical source to produce OH radicals. OD radicals were produced in a similar fashion using the D + $NO_2$ → OD + NO reaction, producing D atoms from a microwave discharge of $D_2$ in He.

For the RF detection of OH radicals, the radiation source was a lamp consisting of a flow of a $He/H_2O$ mixture, which was excited using microwave radiation. OH radicals were detected using the $A^2\Sigma(v=0)\Sigma \rightarrow X^2\Pi(v=0)$ transition near 309 nm. For the LIF system, OH radicals were excited using the A–X(1, 0) band via the $Q_1(1)$ transition near 282 nm using a 20 Hz Nd:YAG pumped dye laser (Lamda Physik). OD radicals were also excited using the A–X (1, 0) band via the $Q_1(1)$ transition at 287.6 nm. Darkened baffles and light traps fitted on the opposite side of the detector were used to reduce background scatter in the chamber. A photomultiplier tube (Hamamatsu H6180-01) equipped with photon counting electronics at a right angle to the radiation source was used to detect the OH or OD fluorescence. An interference filter centered at 308 nm (Esco products) with a 10 nm bandpass and 20% transmission was used to isolate the OH or OD fluorescence. The system sensitivity for OH was $1 \times 10^{-8}$ counts $s^{-1}$ $cm^3$ $molecule^{-1}$ calibrated using the $H + NO_2 \rightarrow OH + NO$ reaction. With a typical background of 300–400 counts $s^{-1}$, a detection limit of $3 \times 10^9$ molecules $cm^3$ (S/N = 1, 10 s integration) was achieved. Similarly, the detection limit for OD was determined to be $8 \times 10^9$ molecules $cm^{-3}$. For these experiments, an initial OH or OD concentration of approximately $3 \times 10^{11}$ molecule $cm^{-3}$ was used.

Heterogeneous loss of OH onto the reactor wall was observed with addition of acetone to the reactor, as preliminary experimental pseudo-first-order decays of OH were non-linear, leading in lower than expected signals of OH as the reaction time was increased and resulting in large positive intercepts (greater than 10 $s^{-1}$) on the second-order plots. The loss is thought to occur when OH undergoes heterogeneous reaction with acetone adsorbed to the walls of the reactor. This was also evidenced by the very slow recovery of the OH signal when the acetone flow was stopped at the end of each experiment. This is in contrast to the expected behavior due to loss of OH on the movable injector, as the OH signal increases with reaction time due to the removal of the injector from the reaction zone. This behavior has previously been observed in the OH + isoprene [23,24], the Cl + isoprene [25,26], and the OH + α-pinene and OH + β-pinene reactions [27]. However, conditioning the wax coating with high concentrations of fluorine radicals, or the addition of approximately (2–5) $\times 10^{15}$ $cm^{-3}$ of $O_2$ to the reactor, minimized the acetone-catalyzed loss of OH radicals on the wall of the reactor, resulting in linear and reproducible pseudo-first-order decays. The addition of oxygen to the flow reactor appeared to inhibit the heterogeneous loss of acetone on the wall of the flow reactor, but did not affect the measured second-order rate constant.

Acetone and acetone-$d_6$ were purified by several freeze-pump-thaw cycles and 20–25% mixtures were prepared by vacuum distillation. Concentrations of acetone ((1.5–74.0) $\times 10^{13}$ molecule $cm^{-3}$) or acetone-$d_6$ ((0.7–23.3) $\times$ $10^{14}$ molecule $cm^{-3}$) were introduced into the flow cell through the injector and the reaction time varied by changing the position of the injector. Acetone concentrations were determined by measuring the pressure drop in the calibrated volume over time. A run was done without the addition of acetone or acetone-$d_6$ to correct for any loss of radicals on the injector.

In another technique for introducing acetone into the reactor, helium was bubbled through liquid acetone or acetone-$d_6$ and then into the reaction zone. The acetone concentration was measured by its absorption at 254 nm in an adsorption cell with a path length of 10 cm using an absorption cross-section of $3.0 \times 10^{-20}$ $cm^2$ $molecule^{-1}$ [28,29]. The pressure of the absorption cell was monitored with a MKS Baratron capacitance manometer. For these experiments, $NO_2$ was obtained from Matheson in a 1.1% mixture in He. Ultra high purity (99.999%) $H_2$ and $O_2$, and zero grade He (99.995%), were purchased from Indiana Oxygen. Acetone (99.5%) and acetone-$d_6$ (99.9 at.%, D) were obtained from Aldrich.

## 3. Computational methods

All calculations were performed using the Gaussian 03 series of programs [30] on the Indiana University IBM RS/6000 Research SP system. Geometries were optimized using Becke's three parameter hybrid method employing the LYP correction functional (B3LYP) in conjunction with 6-31G(d, p) and 6-311++G(2d, 2p) basis sets. Frequencies for all species were calculated at the B3LYP/6-311++G(2d, 2p) level of theory.

## 4. Experimental results

The experimental conditions for these studies are given in Table 1. The experiments were conducted at 5 Torr with additional measurements conducted at 2 and 3 Torr. The reaction rate constants obtained were independent of pressure for measurements done at 300, 341 and 371 K, and for the OH + acetone reaction were independent of the acetone measurement technique. Pseudo-first-order decay rates ($k^I$) were calculated from a weighted (based on the signal-to-noise ratio of each measurement) linear least-squares fit of the logarithm of the OH fluorescence signal versus reaction time, as determined from the reaction distance under the plug-flow approximation ($k^I_{decay}$), and values of $k^I$ were corrected for axial diffusion and OH loss on the movable injector as follows [31]:

$$k^I = k^I_{decay}\left(1 + k^I_{decay}\frac{D}{v^2}\right) - k_{injector} \quad (3)$$

Table 1
Summary of experimental conditions

| Item | Conditions |
|---|---|
| [Acetone] | (0.15–7.4) $\times 10^{14}$ molecule $cm^{-3}$ |
| [Acetone-$d_6$] | (0.7–28) $\times 10^{14}$ molecule $cm^{-3}$ |
| Pressure range | 1.9–5.1 Torr |
| Flow velocity | 9.39–10.3 m $s^{-1}$ |
| Carrier gas | He, He w/10% $O_2$ |
| OH concentration | $<3 \times 10^{11}$ molecule $cm^{-3}$ |
| $O_2$ concentration | (0–5) $\times 10^{16}$ molecule $cm^{-3}$ |
| Diffusion coefficient | OH in He, 0.145 $T^{2/3}$ P Torr $cm^2$ $s^{-1}$ |
| First-order wall removal rates | $<10$ $s^{-1}$ |

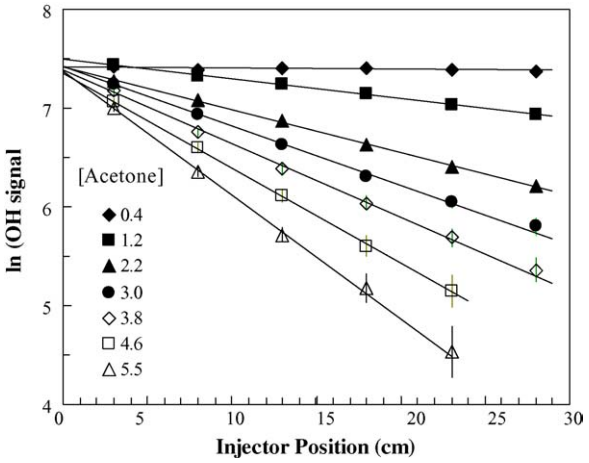


Fig. 1. First-order plot for the OH + acetone reaction at 300 K and 5 Torr. Acetone concentrations are in units of $10^{14}$ molecule $cm^{-3}$. Error bars represents $2\sigma$ uncertainty.

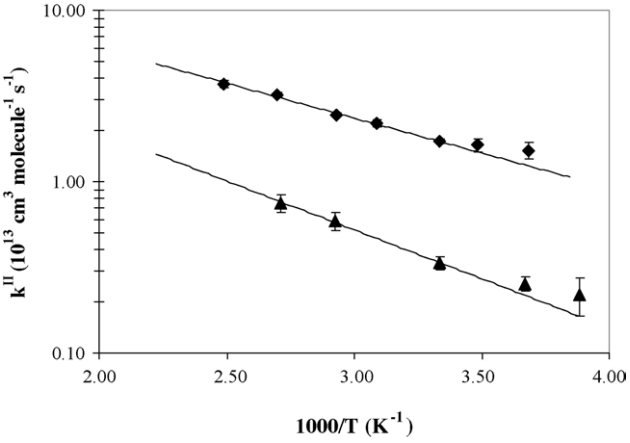


Fig. 3. Arrhenius plot for the OH + acetone and acetone-$d_6$ reactions between 258 and 402 K. Solid diamonds represent acetone data. Solid triangles represent acetone-$d_6$ data. Lines are weighed fit of the data above 300 K.

where $D$ is the diffusion coefficient for OH, $\nu$ the average bulk gas flow velocity, and $k_{\text{injector}}$ is the rate of loss of OH onto the movable injector, measured in the absence of acetone. Fig. 1 shows typical pseudo-first-order plots for the OH + acetone reaction at 5 Torr and 300 K. The pseudo-first-order rate constants were plotted against the acetone concentration to obtain the second-order rate constant.

### 4.1. OH + acetone

Fig. 2 shows the second-order plot at 300 K for the OH + acetone reaction at 300 K. From these experiments the second-order rate constant for OH + acetone at 300 K was determined to be $(1.73 \pm 0.06) \times 10^{-13}$ $cm^3$ $molecule^{-1}$ $s^{-1}$. The error is twice the standard deviation from the weighted fit of the data, with the weights based on the precision of each measurement. This value is independent of pressure between 2 and 5 Torr, and is in good agreement with the recent measurements by Vasvari et al. [12], Wollenhaupt et al. [10], Gierczak et al. [13], Le Calve et al. [32], Raff et al. [20], and Yamada et al. [14] who obtained values of $(1.73 \pm 0.10) \times 10^{-13}$ and $(1.73 \pm 0.09) \times 10^{-13}$ $cm^3$ $molecule^{-1}$ $s^{-1}$, $(1.77 \pm 0.16) \times 10^{-13}$, $(1.87 \pm 0.15) \times 10^{-13}$ $cm^3$ $molecule^{-1}$ $s^{-1}$, $(1.86 \pm 0.13) \times 10^{-13}$ and $(1.56 \pm 0.08) \times 10^{-13}$ $cm^3$ $molecule^{-1}$ $s^{-1}$, respectively. Vasvari et al.'s measurement was done at approximately 3 Torr using discharge-flow (DF) with laser induced fluorescence (LIF) and resonance fluorescence (RF) detection [12], while Wollenhaupt et al.'s measurement was done between 20 and 100 Torr using pulsed laser photolysis (PLP) with detection of OH by pulsed laser induced fluorescence and resonance florescence (LIF) [10]. Gierczak et al. [13], Le Calve et al. [32], and Yamada et al. [14] used PLP and LIF detection at pressures of between 25 and 100 Torr, 300 and 735 Torr, respectively. Raff et al. [20] did a relative study at 735–750 Torr with online mass spectrometry detection of reactants using $C_2H_4F_2$ as the reference compound.

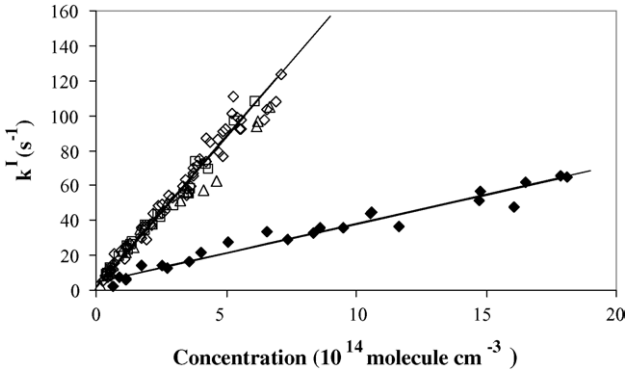


Fig. 2. Second-order plot for the OH + acetone and acetone-$d_6$ reactions at 300 K and 5 Torr. The open symbols represent results for acetone at 2 (□), 3 (△) and 5 (◊) Torr. The solid diamonds represent acetone-$d_6$ data at 5 Torr.

The temperature dependence of the rate constant for the OH + acetone reaction was measured between 271 and 402 K and a plot of the measured rate constant versus inverse temperature (Table 2), is shown in Fig. 3. A weighted fit of the measured rate constants (based on the precision of each measurement) above room temperature results in the following Arrhenius expression: $(3.92 \pm 0.81) \times 10^{-12}$ $\exp((-938 \pm 70)/T)$. This corresponds to an activation energy of $(1.86 \pm 0.14)$ kcal $mol^{-1}$. A similar value of $(1.72 \pm 0.21)$ kcal $mol^{-1}$ was obtained from a weighted fit of all the data in the temperature range studied.

Studies done by Gierczak et al. [13] and Wollenhaupt et al. [10] have shown that below 260 K, the rate constant becomes independent of temperature, approaching a value of $1.4 \times 10^{-13}$ $cm^3$ $molecule^{-1}$ $s^{-1}$. As can be seen from Fig. 3, the rate constants measured in this study below room temperature does begin to exhibit similar behavior. Unfortunately, increased heterogeneous effects at these low temperatures prevented measurements below 270 K. Fig. 4 gives a plot of the temperature dependence of the rate constants obtained in this study for the OH + acetone reaction, and compares these rate constants with previous measurements. As can be seen from this plot the low pressure data reported here is in excellent agreement with previous measurements and with the current recommendation.

Table 2
Summary of experimental results

| $T$ (K) | [Acetone] ($\times 10^{14}$ molecules cm$^{-3}$) | Rate constant ($\times 10^{-13}$ cm$^3$ molecule$^{-1}$ s$^{-1}$) | Pressure (Torr) | Number of experiment |
|---|---|---|---|---|
| OH + acetone | | | | |
| 271 ± 2 | 0.69–5.35 | 1.52 ± 0.12 | 5 | 29 |
| 287 ± 2 | 0.28–6.07 | 1.64 ± 0.14 | 5 | 25 |
| 300 ± 2 | 0.15–7.11 | 1.73 ± 0.06 | 2–5 | 106 |
| 325 ± 2 | 0.74–5.00 | 2.18 ± 0.10 | 5 | 28 |
| 341 ± 2 | 0.17–5.30 | 2.46 ± 0.06 | 2–5 | 71 |
| 342 ± 4 | 0.15–5.35 | 2.54 ± 0.14 | 5 | 34 |
| 371 ± 2 | 0.13–4.95 | 3.11 ± 0.14 | 2–5 | 61 |
| 402 ± 2 | 0.48–3.39 | 3.73 ± 0.14 | 5 | 28 |
| OH + acetone-$d_6$ | | | | |
| 258 ± 2 | 0.73–27.7 | 0.219 ± 0.054 | 5 | 16 |
| 271 ± 2 | 1.32–22.1 | 0.253 ± 0.024 | 5 | 20 |
| 300 ± 2 | 0.66–18.1 | 0.336 ± 0.032 | 5 | 25 |
| 342 ± 2 | 0.89–16.4 | 0.590 ± 0.074 | 5 | 12 |
| 369 ± 2 | 2.16–15.5 | 0.751 ± 0.091 | 5 | 16 |
| OD + acetone | | | | |
| 300 ± 2 | 0.9–7.4 | 2.87 ± 0.22 | 5 | 24 |
| OD + acetone-$d_6$ | | | | |
| 300 ± 2 | 1.9–16 | 0.369 ± 0.012 | 5 | 20 |

### 4.2. OH + acetone-$d_6$

Fig. 2 also shows the second-order plot for the OH + acetone-$d_6$ reaction at 300 K and 5 Torr, and from this data a rate constant of $(3.36 \pm 0.32) \times 10^{-14}$ cm$^3$ molecule$^{-1}$ s$^{-1}$ was obtained using the reservoir system for measuring acetone-$d_6$ concentrations. The reported error is twice the standard deviation for the weighted fit of the rate constant data. This result is in excellent agreement with the values of $(3.00 \pm 0.04) \times 10^{-14}$ cm$^3$ molecule$^{-1}$ s$^{-1}$ obtained by Gierczak et al. [13] at 295 K and 50 Torr, the value of $(3.32 \pm 0.73) \times 10^{-14}$ cm$^3$ molecule$^{-1}$ s$^{-1}$ reported by Raff et al. at 293 K and 1 atm [20], and the value of $(3.24 \pm 0.23) \times 10^{-14}$ cm$^3$ molecule$^{-1}$ s$^{-1}$ reported by Farkas et al. at 298 K and 3 Torr [21]. However, the rate constant reported here is larger than the value of $(2.29 \pm 0.32) \times 10^{-14}$ cm$^3$ molecule$^{-1}$ s$^{-1}$ obtained by Yamada et al. [14] at 730 Torr. The OH + acetone-$d_6$ reaction also showed no pressure dependence between 2 and 5 Torr.

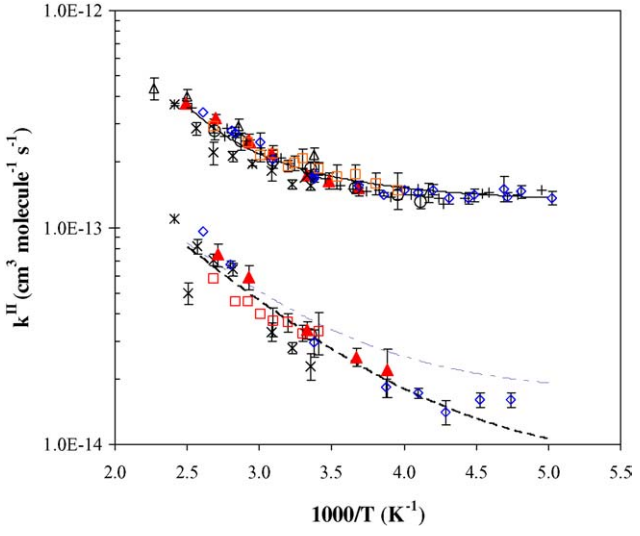


Fig. 4. Arrhenius plot for the OH + acetone and the OH + acetone-$d_6$ reactions. The upper symbols represents data for the OH + acetone reaction: this work (▲),Wallington and Kurylo [8] (△), Le Calve et al. [32] (◯),Wollenhaupt et al. [10] (+),Vasvari et al. [12] (×), Yamada et al. [14] (*), Gierczak et al. [13] (◊), and Raff et al. [20] (□). The solid line represents the calculated rate constant based on the mechanism proposed by Talukdar et al. [17] using the ab initio calculated energies and frequencies (see text). The lower symbols represents data for the OH + acetone-$d_6$ reaction: this work (▲), Gierczak et al. [13] (◊), Yamada et al. [14] (*), Raff et al. [20] (□), and Farkas et al. [21] (◯). The dashed line represents the calculated rate constant for the OH + acetone-$d_6$ reaction based on the abstraction mechanism proposed by Talukdar et al. [17]. The dot-dashed line includes the OH addition rate constant of Raff et al. [20] to the calculated OH + acetone-$d_6$ reaction rate constant.

In contrast to the acetone results, the OH + acetone-$d_6$ rate constant obtained by introducing acetone-$d_6$ using the bubbler system at 300 K was approximately 2 times the value obtained with the reservoir system over the entire temperature range studied. This difference could be due to reactive impurities that were not removed in the purification process in the acetone-$d_6$ which could interfere with the rate constant measurement given the higher concentrations of acetone-$d_6$ required relative to the OH + acetone reaction. Another possibility is the formation of aerosols in the bubbler system due to the higher concentrations of acetone-$d_6$ required, leading to an incorrect determination of the gas-phase acetone-$d_6$ concentration. Another possibility is an error in the absorption cross-section used for acetone-$d_6$. For these experiments, an absorption cross-section at 254 nm of $(2.40 \pm 0.03) \times 10^{-20}$ cm$^2$ molecule$^{-1}$ was used, determined by allowing varying amounts of pure acetone-$d_6$ to enter the absorption cell and measuring both the pressure and the absorption signal. No previous measurements of the absorption cross-section for acetone-$d_6$ at 254 nm have been reported. However, Rao and Murthy [33] found that the ratio of the intensity of acetone-

$d_6$ to acetone absorption ($I_d/I_h$) to be 0.79 at the peak of each (275.6 nm for acetone and 279.3 nm for acetone-$d_6$). This ratio was consistent with our measurements of the absorption cross-section of acetone-$d_6$ relative to that for acetone at 254 nm. In addition, the cross-section of acetone-$d_6$ was also measured at 185 nm and a value of $(4.03 \pm 0.06) \times 10^{-18}$ cm$^2$ molecule$^{-1}$ was obtained, in excellent agreement with the reported value of $(4.01 \pm 0.06) \times 10^{-18}$ cm$^2$ molecule$^{-1}$ by Gierczak et. al. [13]. Measurements of the OH + acetone-$d_6$ rate constant using absorption at 185 nm were consistent with the measurements using absorption at 254 nm, giving additional confidence in our cross-section measurement for acetone-$d_6$ at 254 nm. These results suggest that the difference between the measurements of the rate constant using the reservoir system and the bubbler system for acetone-$d_6$ is not due to an error in the cross-section measurements. For these measurements, only the results obtained using the reservoir system were used.

The Arrhenius plot for the OH + acetone-$d_6$ reaction is also shown in Fig. 3. The weighted fit of the data above 300 K (with the weights based on the precision of each measurement) yields the following Arrhenius expression: $(2.68 \pm 0.55) \times 10^{-12}$ exp$((-1310 \pm 70)/T)$. Similar to the OH + acetone reaction, Gierczak et al. [13] found that the OH + acetone-$d_6$ reaction also displayed non-Arrhenius behavior at low temperature. As shown in Fig. 3, the low pressure rate constants measured in this study for this reaction below 300 K also begin to show similar behavior. These measurements of the temperature dependence of the OH + acetone-$d_6$ reactions are also in reasonable agreement with the measurements of Gierczak et al. [13], Yamada et al. [14], Raff et al. [20], and Farkas et al. [21] as shown by the lower set of symbols in Fig. 4.

### 4.3. OD + acetone and acetone-$d_6$

From these experiments, the second-order rate constant for the OD + acetone reaction at 5 Torr and 300 K was determined to be $(2.87 \pm 0.22) \times 10^{-13}$ cm$^3$ molecule$^{-1}$ s$^{-1}$, in fair agreement with the value of $(2.07 \pm 0.14) \times 10^{-13}$ cm$^3$ molecule$^{-1}$ s$^{-1}$ obtained by Gierczak et al. [13], also at 5 Torr and 300 K. The second-order rate constant for the OD + acetone-$d_6$ reaction was found to be $(3.69 \pm 0.12) \times 10^{-14}$ cm$^3$ molecule$^{-1}$ s$^{-1}$, which is in good agreement with the value of $(3.26 \pm 0.16) \times 10^{-14}$ cm$^3$ molecule$^{-1}$ s$^{-1}$ reported by Gierczak et al. The error is twice the standard deviation for the weighted fit of the data, with the weights based on precision of the data.

## 5. Discussion

Recent quantum mechanical calculations have suggested that H-abstraction in the OH + acetone reaction likely occurs via a hydrogen bonded pre-reactive complex [34] with a stabilization energy of approximately 5–6 kcal mol$^{-1}$ at temperatures below 400 K [14,15,35]. Above 450 K, a direct abstraction mechanism is expected to dominate [14]. A schematic of this mechanism as proposed by Talukdar et al. [17] is shown in Fig. 5. The first step in this mechanism involves the formation of an excited OH-acetone complex ($k_a$), which can either dissociate to reform the reactants ($k_{-a}$), react to form the products ($k_b$), or be collisionally stabilized to form the thermalized OH-acetone complex ($k_c$ [M]). The thermalized complex can be collisionally activated to form the excited complex ($k_{-c}$ [M]) or react to form products ($k_d$). The large kinetic isotope effect may be the result of the influence of quantum mechanical tunneling on $k_b$ and $k_d$ [14,17].

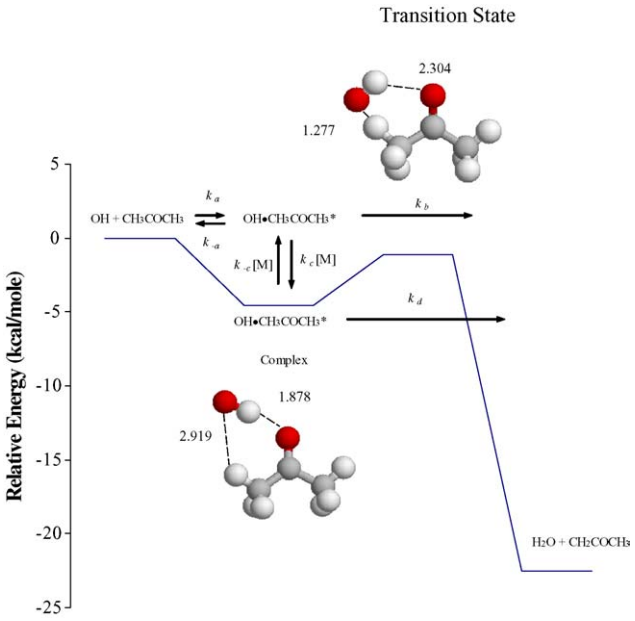


Fig. 5. Schematic mechanism for the hydrogen abstraction channel for the OH + acetone reaction with the individual rate constants indicated (see text). Zero-point corrected relative energies and structures were calculated at the B3LYP/6-311++(2d, 2p) level of theory. Indicated bond lengths are in Å.

The kinetic isotope effect ($k_{acetone}/k_{acetone\text{-}d_6}$)for the OH + acetone reaction varied in our low pressure experiments from a high of 6.0 at 271 K to a low of 4.2 at 368 K, with a value of $(5.1 \pm 0.2)$ at 300 K. A secondary kinetic isotope effect ($k_{OH}/k_{OD}$) of $(0.6 \pm 0.23)$ for the reactions of OH and OD with acetone was observed, as well as a secondary kinetic isotope effect ($k_{OH}/k_{OD}$) of $(0.92 \pm 0.34)$ for the reactions of OH and OD with acetone-$d_6$, in reasonable agreement with those observed by Gierczak et al. [13]. These secondary kinetic isotope effects are consistent with an H-abstraction mechanism, with the larger value of the OD rate constants likely due to the changes in the low frequency vibrations increasing the density of states in a bent transition state to a greater extent than that between OH and OD [36]. No appreciable concentrations of OD were measured from the OH + acetone-$d_6$ reaction at room temperature, suggesting that isotopic exchange through the OH-acetone-$d_6$ complex was not occurring to a significant extent under the conditions of these experiments. The agreement between these low pressure measurements with measurements at higher pressures suggests that H-abstraction is the primary mechanism for this reaction over this temperature range, and is also consistent with a mechanism involving a pre-reactive complex with a small stabilization energy, resulting in rates of stabilization and tunneling factors that are independent of pressure. In contrast, Farkas et al. [21] suggest the observed kinetic isotope effect is not inconsistent with a mechanism that involves both addition and abstraction,

Table 3
Energies, zero-point energies (hartrees), and zero-point corrected relative energies (kcal mol$^{-1}$) for hydrogen abstraction in the OH + acetone reaction

| Structure | B3LYP/6-31G(d, p) | | | B3LYP/6-311++G(2d, 2p) | | |
|---|---|---|---|---|---|---|
| | Energy | ZPE | $E_{rel}$ | Energy | ZPE | $E_{rel}$ |
| OH + acetone | −268.89270 | 0.09216 | 0.0 | −268.98068 | 0.09168 | 0.0 |
| Complex | −268.90810 | 0.09559 | −7.52 | −269.00017 | 0.09470 | −4.58 |
| TS | −268.89440 | 0.09021 | −2.30 | −268.98947 | 0.08954 | −1.09 |
| OH + acetone-$d_6$ | −268.89270 | 0.07320 | 0.0 | −268.99001 | 0.07292 | 0.0 |
| Complex-$d_6$ | −268.90810 | 0.07652 | −7.59 | −269.00017 | 0.07574 | −4.61 |
| TS-$d_6$ | −268.89440 | 0.07300 | −1.20 | −268.98947 | 0.07239 | 0.0 |

as hydrogen abstraction mechanism involving an intermediate complex might lead to a larger kinetic isotope effect similar to that observed for the OH + $HNO_3$ reaction.

In order to determine whether the observed primary kinetic isotope effect for the OH + acetone reaction is consistent with a mechanism involving hydrogen abstraction through an intermediate complex, the structures of the reactants, hydrogen-bonded complex and hydrogen abstraction transition state were optimized at both the B3LYP/6-31G(d, p) and B3LYP/6-311++G(2d, 2p) levels of theory, and the resulting energies and frequencies were used in conjunction with RRKM theory to calculate the overall kinetic isotope effect for this reaction as a function of temperature. The results of the ab initio energy calculations are summarized in Table 3 for the reactants, complex, and the hydrogen abstraction transition state. The resulting structure, vibrational frequencies (see Table 4), and zero-point corrected energies for the OH-acetone complex calculated at the B3LYP/6-311++G(2d, 2p) are similar to the results of Aloisio and Francisco using the same level of theory [34]. The B3LYP/6-311++G(2d, 2p) structure and relative energies of the complex and hydrogen abstraction transition state are similar to the B3LYP/6-311++G(d, p) (−4.72 and −0.55 kcal mol$^{-1}$) and CCSD(T)/6-311++G(2d, 2p) (−5.24 and +3.88 kcal mol$^{-1}$) results of Vandenberk et al. [15], the CCSD(T)/6-311G(d, p)//MP2/6-31G(d, p) results of Vasvari et al. (−6.28 and +3.99 kcal mol$^{-1}$) [12], and the CBS-QB3 calculated energies at the B3LYP/6-311G(d, p) optimized geometries of Yamada et al. [14]. Although the B3LYP/6-31G(d, p) results suggest that the hydrogen abstraction transition state is higher in energy than the reactants, similar to the B3LYP/6-31G(d) results of Masgrau et al. [19], the B3LYP/6-311++G(2d, 2p) results suggest that the transition state is slightly below the energy of the reactants, although the method may underestimate the barrier height for hydrogen abstraction reactions [15,37]. The CCSD(T) results of Vandenberk et al. and Vasvari et al., which predict a positive barrier for hydrogen abstraction, may overestimate the energy of the transition state since they are both single point energy calculations at a geometry optimized at a lower level of theory [15]. However, the CBS-QB3//B3LYP/6-311G(d, p) transition state energies of Yamada et al. determined using the "IRC-max" method results in a barrier of approximately 2 kcal mol$^{-1}$, similar to the experimental activation energy [14]. This value may be more realistic, as it avoids problems associated with poorly characterized single-point transition state structures [14]. However, for simplicity the B3LYP/6-311++G(2d, 2p) energies and uncorrected frequencies were used in the RRKM calculations for the estimation of the kinetic isotope effect for the OH + acetone reaction.

Table 4
Calculated frequencies (in cm$^{-1}$) for species involved in the OH + acetone reaction

| Species | B3LYP/6-31G(d, p) | B3LYP/6-311++G(2d, 2p) |
|---|---|---|
| OH | 3709 | 3720 |
| Acetone | 3166, 3165, 3108, 3101, 3047, 3041, 1822, 1502, 1482, 1480, 1473, 1399, 1396, 1239, 1121, 1086, 888, 888, 785, 531, 486, 376, 136, 41 | 3147, 3146, 3091, 3083, 3040, 3033, 1779, 1493, 1476, 1470, 1466, 1392, 1392, 1237, 1122, 1087, 890, 889, 782, 536, 491, 380, 131, 27 |
| OH-acetone complex | 3492, 3170, 3167, 3112, 3104, 3050, 3043, 1791, 1504, 1485, 1479, 1472, 1409, 1401, 1261, 1128, 1100, 905, 893, 798, 685, 554, 511, 486, 393, 186, 149, 126, 80, 28 | 3509, 3151, 3146, 3095, 3088, 3044, 3037, 1760, 1496, 1477, 1471, 1466, 1400, 1398, 1251, 1126, 1092, 899, 896, 792, 638, 552, 494, 474, 388, 170, 133, 47, 40, 36 |
| OH-acetone TS | 3679, 3167, 3163, 3108, 3088, 3045, 1782, 1534, 1486, 1474, 1446, 1395, 1252, 1167, 1111, 1093, 953, 908, 857, 795, 690, 525, 491, 435, 337, 280, 163, 129, 46, 1349*i* | 3704, 3146, 3143, 3091, 3074, 3037, 1752, 1478, 1468, 1460, 1429, 1388, 1239, 1185, 1107, 1100, 937, 893, 860, 778, 692, 528, 498, 409, 336, 299, 128, 117, 28, 1272*i* |
| Acetone-$d_6$ | 2348, 2346, 2300, 2294, 2191, 2186, 1814, 1255, 1110, 1081, 1070, 1064, 1061, 1024, 984, 899, 716, 694, 674, 477, 403, 315, 101, 30 | 2333, 2331, 2886, 2280, 2185, 2180, 1770, 1242, 1107, 1075, 1063, 1059, 1056, 1025, 985, 898, 715, 694, 677, 484, 408, 319, 97, 20 |
| OH-acetone-$d_6$ complex | 3492, 2351, 2349, 2302, 2295, 2193, 2187, 1780, 1271, 1119, 1083, 1070, 1062, 1061, 1033, 990, 906, 727, 708, 682, 679, 504, 504, 408, 331, 182, 120, 108, 68, 23 | 3509, 2336, 2332, 2289, 2283, 2188, 2182, 1750, 1256, 1115, 1077, 1064, 1057, 1056, 1030, 990, 903, 723, 704, 686, 632, 505, 470, 410, 327, 167, 100, 37, 36, 32 |
| OH-acetone-$d_6$ TS | 3679, 2349, 2347, 2299, 2241, 2188, 1776, 1251, 1206, 1100, 1072, 1060, 1036, 974, 942, 849, 836, 733, 688, 664, 620, 485, 437, 407, 300, 208, 159, 94, 42, 988*i* | 3704, 2333, 2331, 2285, 2230, 2182, 1746, 1230, 1151, 1091, 1065, 1054, 1029, 976, 928, 847, 831, 723, 681, 666, 631, 487, 414, 401, 298, 226, 124, 86, 25, 939*i* |

Table 5
Calculated rate coefficients for the individual reactions in the complex–abstraction mechanism for the OH + acetone and OH + acetone-$d_6$ reactions

| Temperature | $K_{eq}$ ($\times 10^3$) | $k_{-a}$ ($\times 10^{10}$ cm$^{-3}$ s$^{-1}$) | $k_b$ ($\times 10^7$ s$^{-1}$) | $k_d$ ($\times 10^4$ s$^{-1}$) | $k$ (cal) ($\times 10^{-13}$ cm$^{-3}$ s$^{-1}$) |
|---|---|---|---|---|---|
| OH + acetone | | | | | |
| 400 | 2.0 | 12.1 | 41.9 | 63.3 | 3.6 |
| 340 | 1.9 | 4.8 | 28.6 | 6.8 | 2.3 |
| 300 | 2.2 | 2.0 | 6.7 | 3.2 | 1.8 |
| 240 | 4.5 | 0.3 | 0.57 | 0.2 | 1.5 |
| 220 | 7.1 | 0.1 | 0.16 | 0.07 | 1.4 |
| 200 | 13.1 | 0.04 | 0.06 | 0.01 | 1.4 |
| OH + acetone-$d_6$ | | | | | |
| 400 | 2.4 | 15.6 | 11.9 | 9.7 | 0.78 |
| 340 | 2.0 | 6.2 | 8.1 | 0.7 | 0.53 |
| 300 | 2.2 | 2.6 | 1.9 | 0.02 | 0.32 |
| 240 | 4.3 | 0.4 | 0.2 | 0.007 | 0.17 |
| 220 | 6.7 | 0.2 | 0.05 | 0.001 | 0.12 |
| 200 | 12.1 | 0.06 | 0.02 | 0.0002 | 0.11 |

Assuming that the intermediate complex is in steady-state, the overall rate constant for the OH + acetone reaction based on the mechanism shown in Fig. 5 can be expressed by [17]:

$$k = k_a \left( \frac{k_b + K_{eq} k_d}{k_{-a} + k_b + K_{eq} k_d} \right) \quad (4)$$

where $K_{eq}$ is the equilibrium constant between the excited and stabilized complex ($k_c/k_{-c}$). Talukdar et al. [17] demonstrated that this mechanism could explain the observed temperature dependence for the OH + acetone reaction using their measured rate constant for removal of OH ($v = 1$) by acetone and acetone-$d_6$ (2.67 and $3.45 \times 10^{-11}$ cm$^3$ molecule$^{-1}$ s$^{-1}$, respectively) for $k_a$. Using these values for $k_a$ at all temperatures, $k_{-a}$ can be estimated as a function of temperature from equilibrium constant for complex formation determined by the stabilization energy and frequencies of the complex and reactants. Values of the equilibrium constant for complex formation varied from $6 \times 10^{-20}$ cm$^3$ molecule$^{-1}$ s$^{-1}$ at 200 K to $2 \times 10^{-22}$ cm$^3$ molecule$^{-1}$ s$^{-1}$, similar to the values reported by Yamada et al. [14].

The value of $K_{eq}$, the equilibrium constant between the excited and stabilized complex ($k_c/k_{-c}$), can be estimated as a function of temperature using RRKM theory [38]:

$$K_{eq} = \frac{k_c}{k_{-c}} = \frac{Q_c}{P(E^*) \exp(-E^*/kT)} \quad (5)$$

In this equation, $Q_c$ is the partition function for the active modes of the complex, and $P(E^*)$ is the number of quantum states near the dissociation threshold $E^*$ determined using a Beyer-Swinehart counting algorithm. For simplicity, only vibrational modes were used in the calculation.

Table 5 shows the estimated values of $K_{eq}$, and $k_{-a}$ calculated at several temperatures for the OH + acetone and OH + acetone-$d_6$ reactions. Similar to the results of Talukdar et al. [17], values of $k_b$ and $k_d$ for the OH + acetone reaction were determined from a fit of Eq. (4) to the observed values for the overall rate constant using these values of $K_{eq}$, and $k_{-a}$. The resulting values of $K_{eq}$, $k_{-a}$, $k_b$ and $k_d$ are similar to that estimated by Talukdar et al., with the main difference resulting from a larger estimate for $K_{eq}$ that shifts the equilibrium between the energized and stable complex towards higher concentrations of the stabilized complex, leading to lower values of $k_d$.

Values of $k_b$ and $k_d$ for the OH + acetone-$d_6$ reaction were then determined from the corresponding values for the OH + acetone reaction by calculating the kinetic isotope effect for these unimolecular dissociation rate constants. The kinetic isotope effect for $k_b$, the rate constant for the formation of products from the energized complex, was estimated using the following expression from RRKM theory [38]:

$$\frac{k_{bH}(E_H^*)}{k_{bD}(E_D^*)} = \frac{W_H(E^+)/\rho_H(E_H^*)}{W_D(E^+)/\rho_D(E_D^*)} \quad (6)$$

In this equation, $W(E^+)$ is the sum of quantum states in the transition state, and $\rho(E^*)$ is the density of states of the excited complex for the OH-acetone and OH-acetone-$d_6$ reactions. Given the uncertainty associated with the barrier height for the transition state, tunneling corrections were not included. Considering only the vibrational modes for simplicity, and using the ab initio calculated frequencies for the complex and the transition state, this equation leads to a estimated kinetic isotope effect for $k_b$ of approximately 3.5.

The kinetic isotope effect for $k_d$, the rate constant for the formation of products from the stabilized complex, was estimated using the RRKM rate constants at the high pressure limit, corrected for quantum mechanical tunneling [38]:

$$\frac{k_{dH}}{k_{dD}} = \frac{\Gamma_H}{\Gamma_D} \frac{(Q^+/Q)_H}{(Q^+/Q)_D} \exp\left\{ \frac{(E_0)_D - (E_0)_H}{kT} \right\} \quad (7)$$

Here $Q^+$ and $Q$ are the partition functions for the active degrees of freedom in the transition state and the stabilized complex, respectively, for the OH-acetone and OH-acetone-$d_6$ complexes, $E_0$ the zero-point corrected barrier height for the transition state relative to the complex, and $\Gamma_H$ and $\Gamma_D$ are the tunneling transmission coefficients for hydrogen and deuterium systems, respectively. The tunneling coefficients were estimated for transmission through an asymmetric one-dimensional Eckart

potential using the ab initio calculated barrier heights and exothermicities of the complexes relative to the transition state and products, and the calculated imaginary frequencies for the OH-acetone and OH-acetone-$d_6$ hydrogen abstraction transition states (1272*i* and 939*i*, respectively) [39]. The resulting calculated kinetic isotope effect for $k_d$ from Eq. (7) varied from approximately 6.5 at 400 K to 83 at 200 K.

The calculated $k_b$, $k_d$ and overall rate constants for the OH + acetone-$d_6$ reaction are shown in Table 5, and the calculated overall rate constants from Eq. (4) are also plotted in Fig. 4 for both the OH + acetone (solid line) and the OH + acetone-$d_6$ reactions (dashed line). As can be seen from this figure, the calculated rate constants as a function of temperature for the OH + acetone-$d_6$ reaction are in good agreement with the observed rate constants, although the calculations tend to underestimate the measured rate constants at the lowest temperatures. Similar results are obtained when the values of $k_b$ and $k_d$ for the OH + acetone reaction estimated by Talukdar et al. [17] are used with the estimated kinetic isotope effects discussed above.

The results of these simplified calculations are consistent with the more detailed variational transition state theory calculations of the kinetic isotope effect of Yamada et al. [14]. Although the good agreement of these simplified calculations with the observed OH + acetone-$d_6$ rate constants may be due to a cancellation of errors, these results suggest that the observed kinetic isotope effect for the OH + acetone reaction is consistent with a hydrogen abstraction mechanism through an intermediate complex, in contrast to recent suggestions that the lower observed kinetic isotope effect for the OH + acetone reaction compared to the OH + $HNO_3$ reaction may be the result of a significant contribution of an OH addition mechanism [21].

These simple calculations do not take into account the potential increased importance of an OH addition channel in the mechanism of the OH + acetone-$d_6$ reaction at low temperature. Although recent results suggest that the OH addition channel leading to the formation of acetic acid contributes to less than 5% of the overall rate constant for the OH + acetone reaction, the recent measurements of the yield of $d_3$-acetic acid from the OH + acetone-$d_6$ reaction by Raff et al. [20] suggest that the rate constant for the addition channel increases with decreasing temperature, resulting in a $d_3$-acetic acid yield of approximately 20% at 283 K. Based on their measurements of the $d_3$-acetic acid yield, Raff et al. derive a rate constant for the OH addition channel of $k_{add}(T) = ((2.2 \pm 2.8) \times 10^{-15})\ \exp[(285 \pm 246)/T]$. Although the negative temperature dependence of this additional channel is in contrast to theoretical predictions for the barrier to OH addition [19], this rate constant is consistent with an overall acetic acid yield of less than 5% for the faster OH + acetone reaction. Including the rate of OH addition to the calculated overall rate constant for the slower OH + acetone-$d_6$ reaction would increase the predicted rate constant at low temperatures (Fig. 4), and may also explain the discrepancy between the observed kinetic isotope effect and the calculated results of Yamada et al. at low temperatures [14]. However, additional measurements of the rate constant for the OH + acetone-$d_6$ reaction at low temperatures as well as additional theoretical studies are needed to confirm these results.

## 6. Summary

Measurements of the kinetics of the OH + acetone and OH + acetone-$d_6$ reactions using discharge-flow techniques at 2–5 Torr and between 258 and 402 K are in excellent agreement with measurements at higher pressures, consistent with a primary mechanism for this reaction involving hydrogen abstraction. RRKM calculations of the kinetic isotope effect for the reaction as a function of temperature based on the energies and frequencies calculated at the B3LYP/6-311++G(2d, 2p) level of theory are consistent with a mechanism involving hydrogen abstraction through an intermediate complex, although the calculations tend to underestimate the rate constant for the OH + acetone-$d_6$ reaction at temperatures near 200 K. An increased contribution of the OH addition channel to the slower OH + acetone-$d_6$ reaction at low temperatures may explain this discrepancy. Additional measurements of the rate constant for the OH + acetone-$d_6$ reaction at low temperatures, as well as additional theoretical studies of the reaction mechanism would help to resolve this discrepancy.

## Acknowledgement

This work was supported by the National Science Foundation (grants ATM-9984152 and ATM-0106705). This work was also supported in part by Shared University Research grants from IBM Inc. to Indiana University.

## References

[1] D.J. Jacob, B.D. Field, E.M. Jin, I. Bey, Q.B. Li, J.A. Logan, R.M. Yantosca, H.B.J. Singh, J. Geophys. Res. 107 (2002), doi: 10.1029/2001JD000694.
[2] H.B. Singh, D. Ohara, D. Herlth, W. Sachse, D.R. Blake, J.D. Bradshaw, M. Kanakidou, P.J. Crutzen, J. Geophys. Res. 99 (1994) 1805–1819.
[3] H. Singh, Y. Chen, A. Tabazadeh, Y. Fukui, I. Bey, R. Yantosca, D. Jacob, F. Arnold, K. Wohlfrom, E. Atlas, F. Flocke, D. Blake, N. Blake, B. Heikes, J. Snow, R. Talbot, G. Gregory, G. Sachse, S. Vay, Y. Kondo, J. Geophys. Res. 105 (2000) 3795–3805.
[4] P.O. Wennberg, T.F. Hanisco, L. Jaegle, D.J. Jacob, E.J. Hintsa, E.J. Lanzendorf, J.G. Anderson, R.S. Gao, E.R. Keim, S.G. Donnelly, L.A. Del Negro, D.W. Fahey, S.A. McKeen, R.J. Salawitch, C.R. Webster, R.D. May, R.L. Herman, M.H. Proffitt, J.J. Margitan, E.L. Atlas, S.M. Schauffler, F. Flocke, C.T. McElroy, T.P. Bui, Science 279 (1998) 49–53.
[5] R.A. Cox, R.G. Derwent, M.R. Williams, Environ. Sci. Technol. 14 (1980) 57–61.
[6] C. Chiorboli, C.A. Bignozzi, A. Maldotti, P.F. Giardini, A. Rossi, V. Carassiti, Int. J. Chem. Kinet. 15 (1983) 579–586.
[7] J.A. Kerr, D.W. Stocker, J. Atmos. Chem. 4 (1986) 253–262.
[8] T.J. Wallington, M.J. Kurylo, J. Phys. Chem. 91 (1987) 5050–5054.
[9] J.F. Bott, N. Cohen, Int. J. Chem. Kinet. 23 (1991) 1017–1033.
[10] M. Wollenhaupt, S.A. Carl, A. Horowitz, J.N. Crowley, J. Phys. Chem. A 104 (2000) 2695–2705.
[11] M. Wollenhaupt, J.N. Crowley, J. Phys. Chem. A 104 (2000) 6429–6438.
[12] G. Vasvari, I. Szilagyi, A. Bencsura, S. Dobe, T. Berces, E. Henon, S. Canneaux, F. Bohr, Phys. Chem. Chem. Phys. 3 (2001) 551–555.
[13] T. Gierczak, M.K. Gilles, S. Bauerle, A.R. Ravishankara, J. Phys. Chem. A 107 (2003) 5014–5020.
[14] T. Yamada, P.H. Taylor, A. Goumri, P. Marshall, J. Chem. Phys. 119 (2003) 10600–10606.

[15] S. Vandenberk, L. Vereecken, J. Peeters, Phys. Chem. Chem. Phys. 4 (2002) 461–466.
[16] G.S. Tyndall, J.J. Orlando, T.J. Wallington, M.D. Hurley, M. Goto, M. Kawasaki, Phys. Chem. Chem. Phys. 4 (2002) 2189–2193.
[17] R.K. Talukdar, T. Gierczak, D.C. McCabe, A.R. Ravishankara, J. Phys. Chem. A 107 (2003) 5021–5032.
[18] E. Turpin, C. Fittschen, A. Tomas, P. Devolder, J. Atmos. Chem. 46 (2003) 1–13.
[19] L. Masgrau, A. Gonzalez-Lafont, J.M. Lluch, J. Phys. Chem. A 106 (2002) 11760–11770.
[20] J.D. Raff, P.S. Stevens, R.A. Hites, J. Phys. Chem. A 109 (2005) 4728–4735.
[21] E. Farkas, I. Szilagyi, S. Dobe, T. Bereces, F. Marta, React. Kinet. Catal. Lett. 80 (2003) 351–358.
[22] S.S. Brown, J.B. Burkholder, R.K. Talukdar, A.R. Ravishankara, J. Phys. Chem. A 105 (2002) 1605–1614.
[23] B. Chuong, P.S. Stevens, J. Phys. Chem. A 104 (2000) 5230–5237.
[24] P. Stevens, D. L'Esperance, B. Chuong, G. Martin, Int. J. Chem. Kinet. 31 (1999) 637–643.
[25] Y. Bedjanian, G. Laverdet, G. Le Bras, J. Phys. Chem. A 102 (1998) 953–959.
[26] J. Stutz, M.J. Ezell, A.A. Ezell, B.J. Finlayson-Pitts, J. Phys. Chem. A 102 (1998) 8510–8519.
[27] B. Chuong, M. Davis, M. Edwards, P.S. Stevens, Int. J. Chem. Kinet. 34 (2002) 300–308.
[28] R.D. Martinez, A.A. Buitrago, N.W. Howell, C.H. Hearn, J.A. Joens, Atmos. Environ. 26 (1992) 785–792.
[29] T. Gierczak, J.B. Burkholder, S. Bauerle, A.R. Ravishankara, Chem. Phys. 231 (1998) 229–244.
[30] M.J. Frisch, G.W. Trucks, H.B. Schlegel, G.E. Scuseria, M.A. Robb, J.R. Cheeseman, J. Montgomery, Jr., T. Vreven, K.N. Kudin, J.C. Burant, J.M. Millam, S.S. Iyengar, J. Tomasi, V. Barone, B. Mennucci, M. Cossi, G. Scalmani, N. Rega, G.A. Petersson, H. Nakatsuji, M. Hada, M. Ehara, K. Toyota, R. Fukuda, J. Hasegawa, M. Ishida, T. Nakajima, Y. Honda, O. Kitao, H. Nakai, M. Klene, X. Li, J.E. Knox, H.P. Hratchian, J.B. Cross, V. Bakken, C. Adamo, J. Jaramillo, R. Gomperts, R.E. Stratmann, O. Yazyev, A.J. Austin, R. Cammi, C. Pomelli, J.W. Ochterski, P.Y. Ayala, K. Morokuma, G.A. Voth, P. Salvador, J.J. Dannenberg, V.G. Zakrzewski, S. Dapprich, A.D. Daniels, M.C. Strain, O. Farkas, D.K. Malick, A.D. Rabuck, K. Raghavachari, J.B. Foresman, J.V. Ortiz, Q. Cui, A.G. Baboul, S. Clifford, J. Cioslowski, B.B. Stefanov, G. Liu, A. Liashenko, P. Piskorz, I. Komaromi, R.L. Martin, D.J. Fox, T. Keith, M.A. Al-Laham, C.Y. Peng, A. Nanayakkara, M. Challacombe, P.M.W. Gill, B. Johnson, W. Chen, M.W. Wong, C. Gonzalez, J.A. Pople, Gaussian 03, Revision B.05, Gaussian Inc., Wallingford, CT, 2004.
[31] C.J. Howard, J. Phys. Chem. 83 (1979) 3–9.
[32] S. Le Calve, D. Hitier, G. Le Bras, A. Mellouki, J. Phys. Chem. A 102 (1998) 4579–4584.
[33] C.N. Rao, A.S.N. Murthy, Proc. Phys. Soc. 87 (1966) 771–773.
[34] S. Aloisio, J.S. Francisco, J. Phys. Chem. A 104 (2000) 3211–3224.
[35] E. Henon, S. Canneaux, F. Bohr, S. Dobe, Phys. Chem. Chem. Phys. 5 (2003) 333–341.
[36] T. Gierczak, R.K. Talukdar, S.C. Herndon, G.L. Vaghjiani, A.R. Ravishankara, J. Phys. Chem. A 101 (1997) 3125–3134.
[37] J.L. Durant, Chem. Phys. Lett. 256 (1996) 595–602.
[38] K.A. Holbrook, M.J. Pilling, S.H. Robertson, Unimolecular Reactions, 2nd ed., John Wiley and Sons, New York, 1996.
[39] H.S. Johnston, J. Heicklen, J. Phys. Chem. 66 (1962) 532–533.